Evaluation of hybrid spindle bearings with nitriding raceway steels under high rotational speeds

Marcus GÄRTNER [ID][1,*]**, Christian BRECHER** [ID][1]**, Stephan NEUS** [ID][1]**, Leonardo CATANA** [ID][2]**,**
Feliciano GRECO [ID][2]**, Guillermo MORALES-ESPEJEL** [ID][3]**, Defeng LANG** [ID][3]

[1] Laboratory for Machine Tools and Production Engineering (WZL), RWTH Aachen University, Aachen, Germany
[2] SKF Industrie S.p.A., Turin, Italy
[3] SKF Research and Technology Development, Houten, Netherlands
*Corresponding author: m.gaertner@wzl.rwth-aachen.de

Abstract

The further development of high-precision bearings regarding higher speeds and load-carrying capacity is becoming increasingly challenging. One approach to meet the increased requirements is to use new high-performance raceway steels. Particularly for a highly stressed lubricant film, where seizure may occur, the bearing material properties can make a key contribution in increasing the lifetime. In the following, the test results of hybrid spindle bearings of type 7008 made of nitriding steel are analysed. The bearings were tested in an endurance run for a constant speed parameter of 2.5 million nd_m and a maximum contact stress of 2,900 MPa at the inner ring contact. The operational behaviour was validated based on the bearing outer ring temperature and the acceleration level in the test rig. A further sample test in endurance runs with an increased speed parameter of 2.8 million nd_m and a maximum contact stress of 3,200 MPa at the inner ring shows that the performance limit of the bearing is even higher than initially assumed. The microscope analyses of the bearing steels after the test show low wear. An analysis of the test conditions in terms of contact stresses, lifetime and the *pv* value illustrates that the bearings can run far above standard conditions. The experimental results show that the operational limits of hybrid spindle bearings with a raceway made of nitriding steels are significantly higher than expected.

1. Introduction

The technical requirements for motor spindles and their bearings are steadily increasing regarding speed capability, load-carrying capacity and lifetime. In the case of machining titanium alloy for applications in the aerospace industry, high cutting forces during the process are acting on the spindle and their bearings, which can lead to early bearing failures [1]. One approach to meet these challenges is to use bearings with higher-performance materials. The use of ceramic balls made of silicon nitride in spindle bearings, so-called hybrid spindle bearings, has proven successful due to their lower

density compared to steel balls and the associated lower centrifugal forces [2]. Besides this, hybrid spindle bearings excel through their superior tribological characteristics, compared with steel bearings [2]. To compare the speed limits of spindle bearings of different sizes the speed parameter is used, which is the product of maximum rotational speed n and the pitch diameter d_m. Typical speed limits of high-precision hybrid spindle bearings today are around a speed parameter of 2.7 million nd_m [3].

Due to high loads and high sliding speeds in the rolling contact, the lubricant film is highly stressed. In case of a sudden failure of the lubricant film, it comes to solid contact between the ball and the raceway, resulting in adhesive wear, which is referred to as seizure [4]. Even if such an influence is not taken into account in the lifetime calculation, it

can nevertheless be assumed that this mechanism occurs more and more with increasing load and speed, which results in a decrease in the lifetime. To estimate the lifetime of the bearings under these conditions accurately, a precise, statistically validated determination of the bearing parameters such as the static load rating C_0, dynamic load rating C and fatigue limit load P_u is necessary [5].

In a new calculation approach, the fatigue strength of various bearing steels could then be determined with the exact material parameters in good agreement with experimental results [6]. In particular, the microstructure of the raceway steels has a strong influence on the fatigue strength under extreme conditions, which was demonstrated by tribometer tests [7]. Furthermore, powder metallurgical steels show good frictional heating resistance under high loads compared to conventional steels, which also has a positive effect on fatigue strength [8]. In recent tests with hybrid bearings manufactured with powder metallurgical raceway steels, the improved speed capability and load-carrying capacity in endurance runs could be demonstrated [9]. In aerospace applications, raceway steels made of *Cronidur 30* have proven their reliability due to their corrosion resistance, better scuffing properties and the associated longer lifetime [10,11].

The various research results generally show that the approach to increase the performance of the bearings made from new types of bearing steels with improved material properties is promising. It has already been shown in the past that the mechanical properties and lifetime of bearings made of nitriding steels can be improved compared to conventional bearings [12,13]. However, the performance limits of hybrid bearings made of nitriding steels in endurance runs have not yet been investigated, which is therefore, the focus of this paper.

2. Experimental methods

The following paragraph describes the test bearings and the composition and properties of the raceway steel. Furthermore, the properties of the test rig and the test conditions are explained before the results of the test runs are discussed.

2.1 Test bearings and material

In this test series, ten prototype hybrid spindle bearings of type 7008 consisting of bearing rings with nitriding steel with a contact angle of 18° were tested in endurance runs. According to the catalogue, the limiting speed of a comparable

bearing type with conventional raceway steel (100Cr6) is 56 krpm ($\triangleq$ 56,000 rotations per minute) at a moderate axial load of 620 N. The test bearings are manufactured with tolerance class 4 in accordance with ISO 492 [14]. The geometry data of the test bearing with a cross-sectional view are shown in Figure 1.
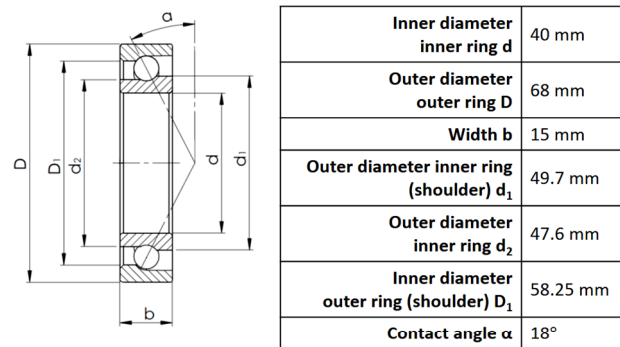

Inner diameter inner ring d	40 mm
Outer diameter outer ring D	68 mm
Width b	15 mm
Outer diameter inner ring (shoulder) d_1	49.7 mm
Outer diameter inner ring d_2	47.6 mm
Inner diameter outer ring (shoulder) D_1	58.25 mm
Contact angle α	18°

Figure 1. Bearing data and geometry

The composition of the raceway steel of the tested bearings compared to the conventional steel 100Cr6 is given in Table 1. The tested bearing steel is heat treated and nitrided, which results in a higher surface hardness and a high adhesive wear resistance [15]. The conventional raceway steel 100Cr6 is also heat treated [16]. The higher element shares of chromium, molybdenum and copper, for instance, provide the tested raceway steel with better corrosion resistance compared to the conventional raceway steel.

Table 1. Properties of the steels [17-19]

		Conventional raceway steel	Tested raceway steel
Chemical composition, wt. %	C	0.9	0.33
	Si	0.3	0.25
	Mn	–	0.55
	P	–	0.02
	Cr	1.5	3.05
	Mo	0.03	0.95
	Ni	–	0.3
	V	–	0.25
	Cu	–	0.1
Hardness HRC		61.4	66.0
Yield strength $R_{p0.2}$, MPa		500	950
Tensile strength R_m, MPa		900	1,150
Elongation at fracture A, %		5	12

Similar to nitrocarburising, nitriding introduces nitrogen into the surface, which increases surface quality, reduces wear coefficients and minimises seizure in the long term [20]. The high-chromium and iron alloy share also increases the diffusion of nitrogen deeper into the material [21]. Furthermore, the tested nitriding steel is characterised by a higher Rockwell hardness, yield strength, tensile strength and elongation at fracture.

2.2 High-speed test rig and test conditions

The bearings were tested on a high-speed rolling bearing test rig, which is shown in Figure 2. This concept is characterised by its high modularity so that bearings of different types and sizes can be tested by minor adjustments to the shaft and housing [22]. The test bearings in the test rig are driven by a motor spindle, which can reach a maximum rotational speed of 60 krpm. For sufficient preload axial forces up to 600 N can be applied to the bearings by a hydraulic force control. The temperature on the bearing outer ring is measured during the test with a resistance temperature sensor.
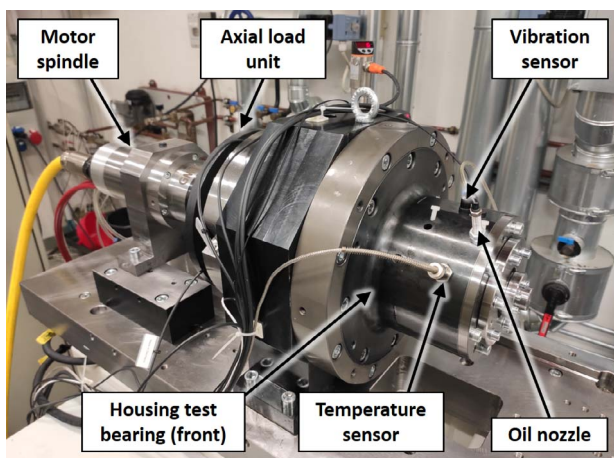

Figure 2. High-speed bearing test rig

The acceleration level is monitored by a uniaxial piezoelectric acceleration sensor MMF KS94C100, for a frequency range of up to 51.2 kHz.

To give an overview, the test rig is shown in its cross-section view and force flux in Figure 3. During operation, two bearings, arranged in an O arrangement, can be tested in parallel. The back bearing is mounted on a sliding seat, which is axially movable. The axial preload force of the hydraulic cylinders is controlled based on the feedback signal of the force sensors so that the preload force is kept on a constant level. The bearing arrangement is a fixed floating arrangement with axial force control.

Like in main tool spindles, the bearings are lubricated with oil-air lubrication with a fine-filtered synthetic spindle bearing oil of viscosity class ISO VG 68. The purity class for the oil tested is 15/13/10 and is defined according to ISO 4406 [23]. In this code the first number stands for the number of particles smaller than 4 µm, the second one is the number of particles smaller than 6 µm and the third one is the number of particles smaller than 14 µm per milliliter of fluid. The front bearing is lubricated by a height-adjustable oil nozzle with a diameter of 1 mm, the oil in the back bearing is injected by an injection ring with two nozzles with a diameter of 0.5 mm. Before each test run, the bearings are pre-lubricated for 12 h that standstill, so that there is a sufficient quantity of oil in the bearing before the test is started. The control interval for the oil fed was 10 s.
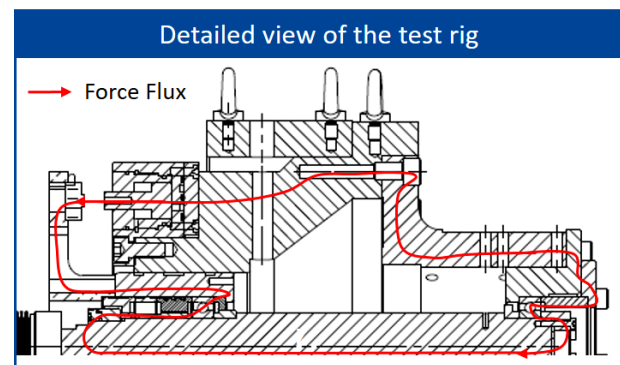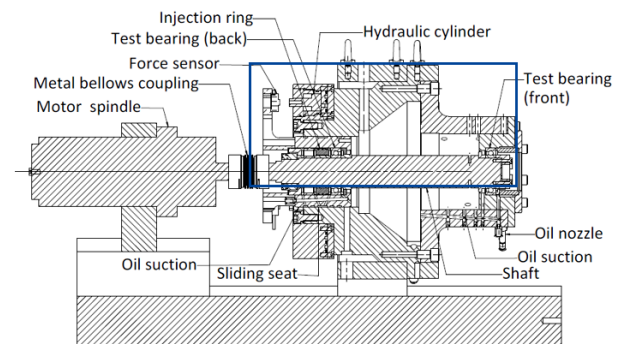

Figure 3. Cross-section of the test rig with force flux

To avoid over-lubrication of the bearings and to remove the stressed oil from the bearing, an oil suction system is provided. To safeguard the results, the first four tests were carried out under the same conditions shown in Table 2. In a sample test (test run 5) with increased speed and load the performance limits were investigated with the last bearing pair, which is also given in Table 2. A sufficient amount of lubricant in the bearing must always be ensured and can prevent failure [24,25]. Therefore, in test run 5, the amount of lubricant was increased to 300 µl/h due to the increased rotational speed and load. The contact stresses

were determined with the shaft bearing software MTPlus, which is described in section 3.1 based on the Hertzian approach.

Table 2. Test condition in the endurance run

Test runs 1 – 4	
Rotational speed n	46 krpm
Speed parameter nd_m	2.5 million
Axial force F_{ax}	3 kN
Maximum contact stress (inner ring) p_{max}	2,900 MPa
Test duration t_d	432 h
Lubricant quantity for each bearing q	240 µl/h
Sample test run 5	
Rotational speed n	52 krpm
Speed parameter nd_m	2.8 million
Axial force F_{ax}	4 kN
Maximum contact stress (inner ring) p_{max}	3,200 MPa
Test duration t_d	460 h
Lubricant quantity for each bearing q	300 µl/h

Due to the high speeds, the shaft and the metal bellows coupling are balanced with the highest balancing quality of G2.5 for the operating speed. At the beginning of the test, the speeds of 2 krpm, 5 krpm and 10 krpm are first approached in a short step run, with a parallel stepwise increase in the preload force from 1, 2 and up to 3 kN. In the last step, the speed is accelerated to 46 krpm within a few seconds to pass through possible critical bearing frequencies quickly and to avoid pre-damage of the bearings. Then the test bearings are operated at a comparatively high speed parameter of 2.5 million nd_m in an endurance run. In the case of test run 5, the speed level of 46 krpm and forces application is approached in the same way as in the tests before and are held for 24 h. Then the axial force is increased to 4 kN and the target speed of 52 krpm is approached, which is kept on a constant level for 430 h. The objective of the tests is to determine the fatigue limit of the new bearing prototypes with the nitriding raceway steel and to estimate the influence of the adhesive wear mechanism of seizure.

2.3 Test results

The operational behaviour of the bearings in the endurance run was validated by the temperature of the outer ring and the acceleration in the test rig. The outer ring temperatures of the five test runs are shown in Figure 4. In general, test runs 1 – 4 were successfully completed, without exceeding the outer ring temperature limit of 90 °C for constant operational conditions. Therefore, it can be assumed that the performance limits of the bearings have not yet been reached under these operational conditions.
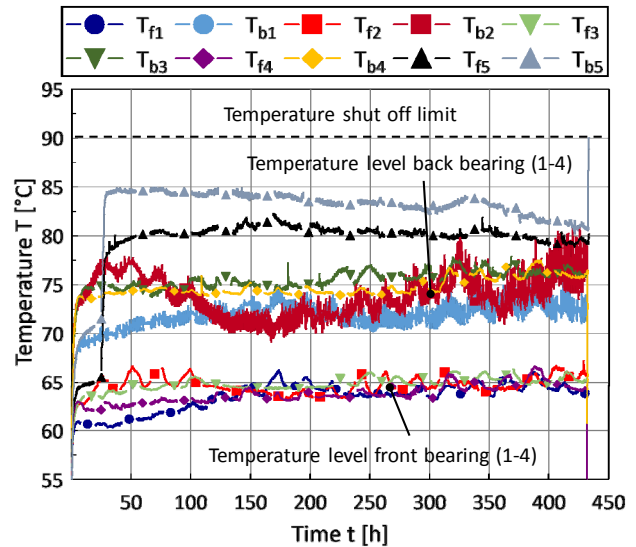
Index: f/b: Position (front/back), i: Test number

Figure 4. Outer ring bearing temperatures

Furthermore, it can be stated that the temperature level of the back bearing is higher in all tests compared to the front bearing. The level of the back bearing is on average about 75 °C, and the front level of the front bearing is about 65 °C. This can be attributed to the poorer heat dissipation in the back bearing, which is surrounded by considerably more housing mass compared to the front bearing. Besides this, slightly different lubrication conditions have to be considered. Since the oil is only fed to the bearing in controlled intervals, the actual amount of lubricant in the bearing can fluctuate slightly, which leads to greater fluctuations in the temperature level due to the high speed of 46 krpm.

In test run 5, the speed parameter was increased to 2.8 million nd_m and a maximum inner ring contact stress of 3,200 MPa. In this case, a steady-state temperature of 83 °C for about 400 h was initially achieved. Subsequently, a sudden temperature rise in the back bearing occurred, which led to a switch-off due to exceeding the temperature limit of 90 °C. This temperature limit is sufficient to investigate the bearings under tough operational conditions, but still uncritical for the bearing [26]. However, macroscopically the damage to the back bearing 5 was not detectable. In addition to the bearing outer ring temperature, the vibration behaviour was measured in the test

rig, so that e.g. dynamic effects can also be detected. The acceleration values from the tests are shown in Figure 5. According to Shannon's theorem, the sampling rate must be at least twice as large as the highest measurable frequency, so that an evaluation in the frequency range is limited to half the sampling frequency.
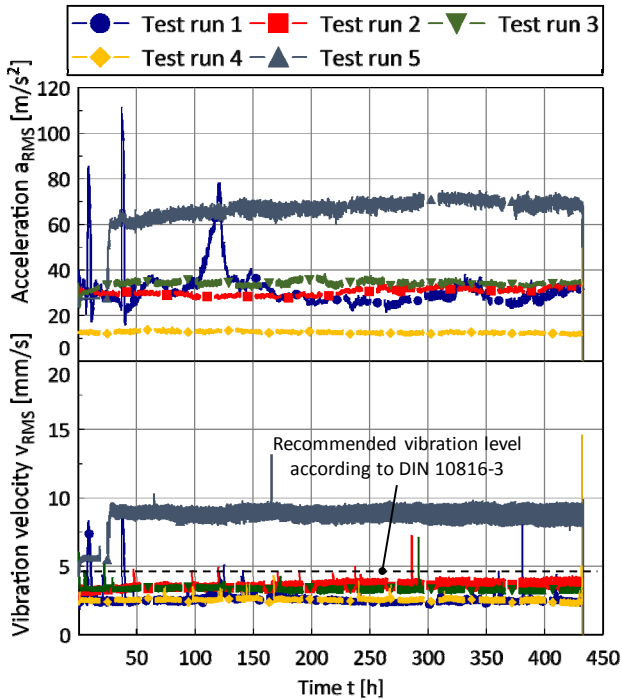

Figure 5. Acceleration and vibration velocities

To measure a wide frequency spectrum, the highest sampling rate of the sensor of 51.2 kHz was used for the investigations. To reduce the amount of data, the acceleration signals are evaluated as a root mean square a_{RMS} (RMS) value for a frequency range from 10 to 25.6 kHz during the test. The RMS value can be calculated with the following formula.

$$a_{RMS} = \sqrt{\frac{1}{\tau} \int_{0}^{\tau} a^2(t)\,\mathrm{d}t} \,. \qquad (1)$$

where τ is the time period, a is the raw acceleration signal and t is the time.

The acceleration levels of test runs $1-3$ are at a comparable level of around 33 m/s², while test run 4 represents an outlier regarding acceleration. In contrast, test run 5 with the higher test conditions values has a higher acceleration level. According to the ISO 10816-3 standard, the vibration velocities in machines are also classified. Therefore, the vibration velocities based on the RMS value were also calculated, which are also shown in Figure 5. The vibration velocities should not permanently exceed a value of 4.5 mm/s as

specified in the standard, which is widely fulfilled in test runs $1-4$ [27].

The vibration signals can also be used to determine the lubrication condition in the bearing [28,29]. An insufficient lubrication condition is then indicated by an increased acceleration level in the test rig. Particularly for test run 1, there are some peaks in the acceleration signal at the beginning. However, the lubricant supply is constant and no corresponding temperature fluctuations can be detected in the temperature measurement. However, in test run 5, the acceleration values are at around 70 m/s² and vibration velocities are at 9 mm/s in a steady state but clearly above the standard limits. Nevertheless, at the failure after about 430 h, there is no acceleration peak, which is consistent with the photos of the bearings after the test, which show nearly no wear. Especially the results of test run 5 reveal that the performance limits of this bearing type with the raceway of nitriding steel are very high with regard to load and speed. Generally, the performance of the bearings regarding temperature and acceleration measurement under permanent and relatively high stresses appears to be good.

2.4 Microscopic analysis of the raceways

Since test runs $1-4$ had an almost constant temperature and acceleration level, no significant wear is expected on the bearings. Nevertheless, it can be assumed, that due to the high speeds and loads, adhesive wear mechanisms occur. Figure 6 shows exemplary microscope views of the inner ring raceways of the front and back bearing of the first test run. The microscope views of the other tested bearings showed similar behaviour. The microscope used for this investigation was Keyence VHX-6000. The brown marks on the raceway indicate oxidation reactions with the lubricant due to the high energy input in the test.
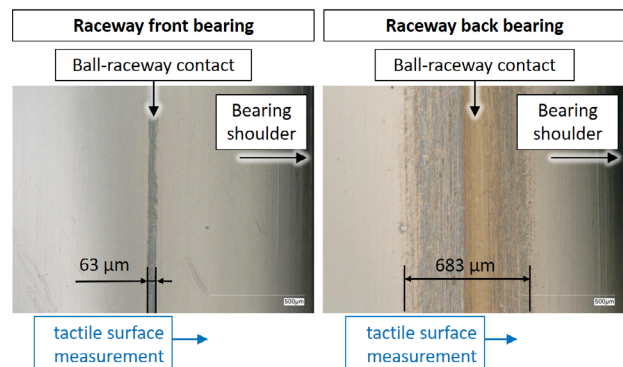

Figure 6. Microscopic view of raceways
(bearings 1 and 2)

The mark on the back bearing is larger compared to the front bearing, which can be attributed to the higher temperature level in the back bearing and the slightly different lubrication conditions compared to the front bearing. In Figure 7 the rolled-up surface profiles from the rolling contact of the first test run are depicted. The measurements were carried out with a contour measurement station Mahr MarSurf XC 20, which has a resolution lower than 1 µm depending on the probe arm. Tactile measurements of the surface profile across the raceway show no wear. On the one hand, this demonstrates that the bearing wear is at an early stage and that it is not detectable based on the measurements.
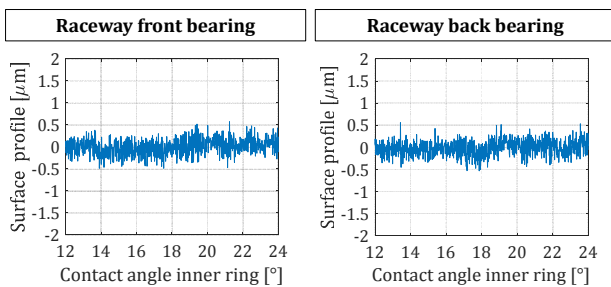

Figure 7. Surface roughness measurements (bearings 1 and 2)

In addition, roughness measurements were taken of the bearings before the test. The measured Ra values of the bearings for the inner and outer ring of the two bearings are shown in Table 3. The relatively low Ra values illustrate the high surface quality of the bearing raceways.

Table 3. Surface roughness measurements (bearings 1 and 2)

|	Ra, µm	
	Inner ring	Outer ring
Bearing 1 (front)	0.016	0.018
Bearing 2 (back)	0.017	0.019

On the other hand, it is evident that the temperature level in the bearing can favour chemical reactions between the raceway and the lubricant. A comparison of the raceways in Figure 6 with the classification in [7] shows that the bearing steel has good micropitting resistance.

3. Validation of the test conditions

In the following section, the test conditions are analysed regarding contact stresses, bearing kinematics, pv value and lifetime. The calculations shall illustrate the level of the loads and speeds in the test.

3.1 Simulation model

To calculate the operating conditions of the test bearings, a simulation model was built using the MATLAB-based software MTPlus. The program enables a holistic calculation of the operating conditions of the bearings, taking into account the influences of shaft and housing [30]. The MTPlus model of the test bench is shown in Figure 8. To build the model, the geometric and mechanical properties of the conversion parts, i.e. shaft, housing and sliding seat and bearings are defined. The housing is coupled to the environment by supports, one with a fixed degree of freedom in the axial direction, the other axially movable to enable thermal expansion of the housing.
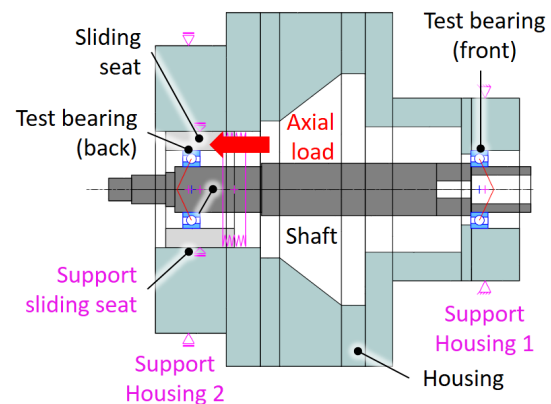
Roughness ring	0.017 µm
Roughness ball	0.011 µm
Equivalent load rating P	4.3 kN
Dynamic load rating C_r	17.8 kN
Static load rating C_{r0}	14.5 KN

Figure 8. MTPlus model of the test rig

The support of the sliding seat enables axial movement. The axial force application is approximated by the preload spring, which also has an almost constant load-displacement characteristic compared to the hydraulic force control. The operational conditions of the bearings are determined by iterative solutions of force equilibrium, which can generally be described by Equation (2).

$$F = K x + C \dot{x} + M \ddot{x}. \tag{2}$$

The force vector for each bearing results from the matrices of the system stiffness K, system damping C and the system mass M as well as from the vectors of displacement x, velocity $\dot{x}$ and acceleration $\ddot{x}$. The bearings are approximated as spring-damper elements and the surrounding parts are simulated by FEM beams. This approach allows us to consider influences from the surrounding

parts on the bearings in the calculation, such as thermal expansion, shaft interferences or fits.

3.2 Contact stresses

To illustrate the loads in the bearings, the contact stresses p for the front bearing for the outer ring (OR) and inner ring (IR) are given in Figure 9 over the length of the Hertzian contact ellipse 2a for the test conditions.
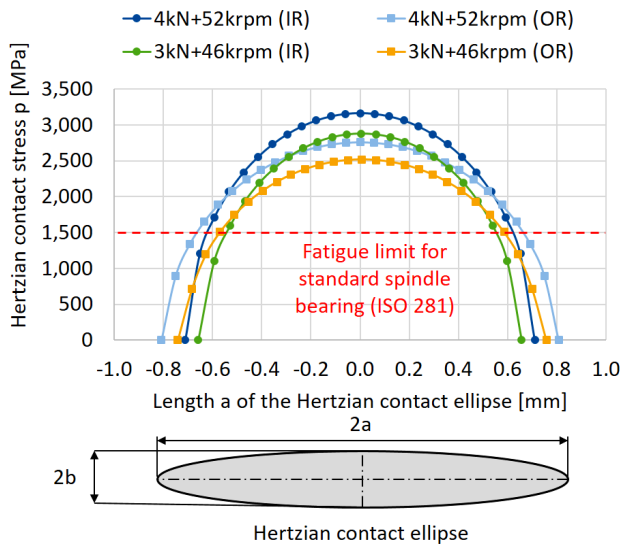

Figure 9. Contact stresses of the front bearing

The locally resolved contact stresses $p(x,y)$ can be calculated with Equation (3) [31].

$$p(x,y) = p_{max} \sqrt{1 - \left(\frac{x}{a}\right)^2 - \left(\frac{x}{b}\right)^2}. \tag{3}$$

The maximum contact stress p_{max} can be determined with the contact force Q by Equation (4).

$$p_{max} = \frac{3Q}{2\pi ab} = \frac{\sum \rho E_{red}}{2\pi ab} \left(\frac{2\delta}{\delta_{Herz} \sum \rho}\right)^{3/2}. \tag{4}$$

In this equation, the curvature sum $\Sigma\rho$ and the deformation can be calculated according to [32]. The coefficient δ_{Herz} can be approximated with a simplified approach for elliptical‑contact deformation [33]. The reduced modulus of elasticity E_{red} is established with Equation (5), which considers the modulus of elasticity E and the Poisson's ratio v of the contact bodies [34].

$$\frac{1}{E_{red}} = \frac{1}{2}\left(\frac{1-v_1^2}{E_1} + \frac{1-v_2^2}{E_2}\right). \tag{5}$$

The results are based on the nominal geometries of the bearings. Due to the higher load

of 4 kN, a larger contact ellipse and contact surface stress are formed compared to the case with 3 kN. As a result of the typically higher osculation Λ at the contact between the radius of the inner ring r_{IR} or outer ring r_{OR} and the radius of the rolling element r_{RE} compared to the outer ring contact, higher contact stresses occur at the inner ring. The equation to calculate the osculation Λ according to [32] is given in Equation (6).

$$\Lambda = \frac{r_{RE}}{r_{IR/OR}}. \tag{6}$$

For the more critical inner ring contact, stresses of 2,900 MPa are achieved for test runs $1-4$, while stresses of up to 3,200 MPa are achieved for the increased axial preload in test run 5. For both operational conditions, the rolling contact stresses are significantly above the fatigue strength limit of 1,500 MPa specified in the ISO 281 standard [35]. Since the tested bearings withstood these critical conditions for 430 h, it is assumed that their fatigue strength is above that of standard bearings.

3.3 Ball kinematics

Another important design parameter is the spin-to-roll ratio ω_s/ω_r, which is depicted for the two operational conditions in Figure 10. Depending on the bearing manufacturer, the limit values can vary. Nevertheless, the spin-to-roll ratios for the front and back bearing can be classified as uncritical for both operating conditions.
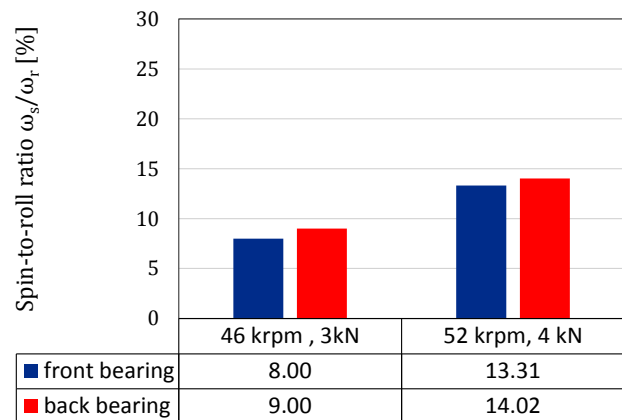

	46 krpm , 3kN	52 krpm, 4 kN
front bearing	8.00	13.31
back bearing	9.00	14.02

Figure 10. Spin-to-roll ratio ω_s/ω_r inner ring contact

However, the high speeds influence friction and wear in the bearing. Due to the load, a deformation of the rolling element occurs, leading to a contact ellipse, which is depicted discretised for the inner ring ball contact in Figure 11. For this contact, the relative velocities can be calculated for the difference between ball velocity v_{ball} and

raceway velocity v_{ir} in the rolling contact according to Equation (7).

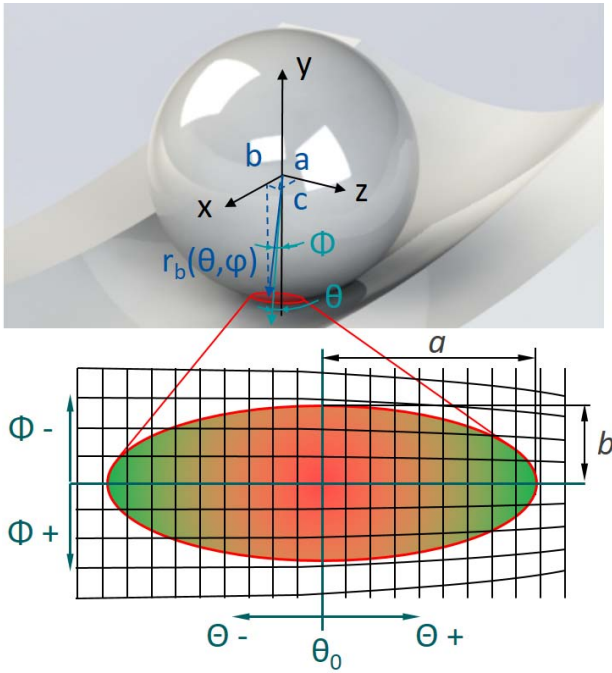$$\vec{v}_{rel} = \vec{v}_{ball} - \vec{v}_{ir}. \tag{7}$$

Figure 11. Discretisation of the ball surface

Depending on the contact ellipse the ball velocity can be expressed with Equation (8). The single velocity components of the ball $v_{b,i}$ result from the angular velocity components of the ball $\omega_{b,i}$ and under the contact flattening in the rolling contact c [36].

$$\vec{v}_{ball} = \begin{pmatrix} v_{b,x} \\ v_{b,y} \\ v_{b,z} \end{pmatrix} = \begin{pmatrix} \omega_{b,y}\,b - \omega_{b,z}\,c \\ -\omega_{b,x}\,b + \omega_{b,z}\,a \\ \omega_{b,x}\,c - \omega_{b,y}\,a \end{pmatrix}. \tag{8}$$

The raceway velocity can be calculated with Equation (9), considering the angular velocity components of the inner ring $\omega_{ir,i}$ and the cage $\omega_{c,i}$ and the pitch diameter d_m.

$$\vec{v}_{ir} = \begin{pmatrix} v_{ir,x} \\ v_{ir,y} \\ v_{ir,z} \end{pmatrix} = \begin{pmatrix} 0 \\ -(\omega_{ir,x} - \omega_{c,x})\left(\dfrac{d_m}{2} + b\right) \\ (\omega_{ir,x} - \omega_{c,x})\,c \end{pmatrix}. \tag{9}$$

Based on these equations the calculated relative speeds v_{rel} at the critical inner ring rolling contact are shown locally resolved in Figure 12. Especially in the areas where the two velocity components are opposite, i.e. in the area of negative relative velocities, the slip is particularly high, resulting in high frictional energy input in these areas.
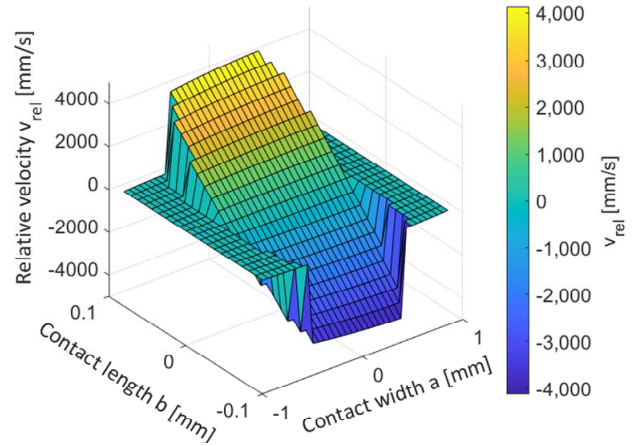

Figure 12. Relative velocities v_{rel} in the rolling contact

3.4 *pv* value

The pv_{rel} value can be determined from the product of locally resolved contact stresses p and relative speed v_{rel}. This value illustrates the energetic input in the rolling contact and can be related to the expected local wear rate. The locally resolved pv_{rel} value is shown in Figure 13 for 52 krpm and 4 kN axial load.
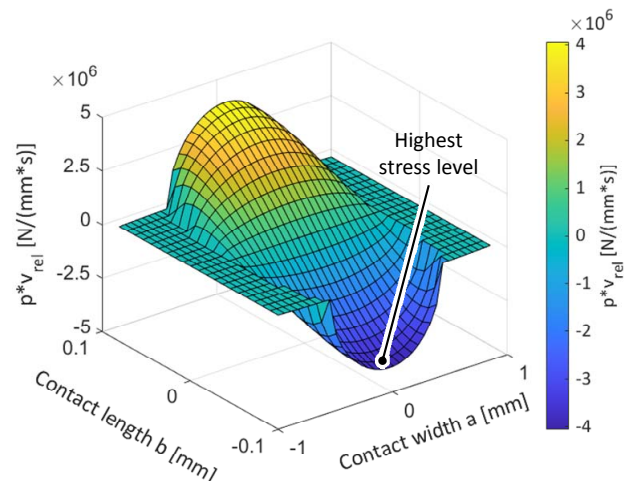

Figure 13. *pv* value for the inner ring in the rolling contact (52 krpm, 4 kN)

In particular, the area with a maximum negative value is heavily stressed due to the slip conditions previously described. A failure of the lubricant film is especially expected in this area.

3.5 Lifetime calculation

The lifetime calculation is an important design parameter for rolling bearings, taking into account the influences of load, speed and lubrication. The calculation can be performed according to the technical specification ISO/TS 16281 [37]. For a rough estimation, the basic rating lifetime L_{10h} can be calculated with the following equation [35]:

$$L_{10h} = \left(\frac{C_r}{P_r} \right)^p. \tag{10}$$

The basic dynamic radial load rating C_r can usually be determined from the manufacturer's bearing data. The exponent depends on the type of rolling contact, for a point contact in ball bearings p = 3, and for a line contact in roller bearings p = 10/3. The radial forces F_r and axial forces F_{ax} applied to the bearing are considered by the dynamic equivalent bearing load P_r, which is determined by the weighting factors X, Y with Equation (11).

$$P_r = X F_r + Y F_{ax}. \tag{11}$$

The reliability a_1 and lubrication influence a_{ISO} are considered in the modified rating lifetime L_{nmh}, which can be calculated with the following equation.

$$L_{nmh} = a_1 \, a_{ISO} \, L_{10h}. \tag{12}$$

The factors can be determined with tables, which can be found in ISO 281 [35]. Since a reliability of 90 % is assumed, factor a_1 is 1. The a_{ISO} factor of 20.11 is quite high. This can be attributed to the high viscosity ratio κ of 4, and because of the high rotational speeds full lubrication conditions can be assumed. Additionally, the characteristic value $(e_c \cdot C_u)/P$ is determined with 0.16. Therefore, the calculated modified lifetime can be higher compared to the basic lifetime. These calculation procedures are also used, e.g. in new prediction approaches to predict wear with neural networks [38].

If the internal load distribution in the bearing is considered, the basic reference rating lifetime L_{10rh} of the ISO specification ISO/TS 16281 can be used. This calculation method considers the shaft tilting, bearing clearance and material influences. In the modified reference rating lifetime L_{nmrh} the lubricant influence a_{ISO} and reliability a_1 are also taken into account. The lifetime according to ISO/TS 16281 for the two preload conditions of 3 and 4 kN is given for an increasing speed in Figure 14. The depicted calculations are just a reference since the ISO approach can not consider the characteristics of the tested hybrid spindle bearings [39]. With increasing rotational speed and load, the lifetime decreases, due to higher centrifugal forces and load cycles. The modified reference rating lifetime is higher compared to the basic reference rating lifetime, due to the consideration of the lubrication film.
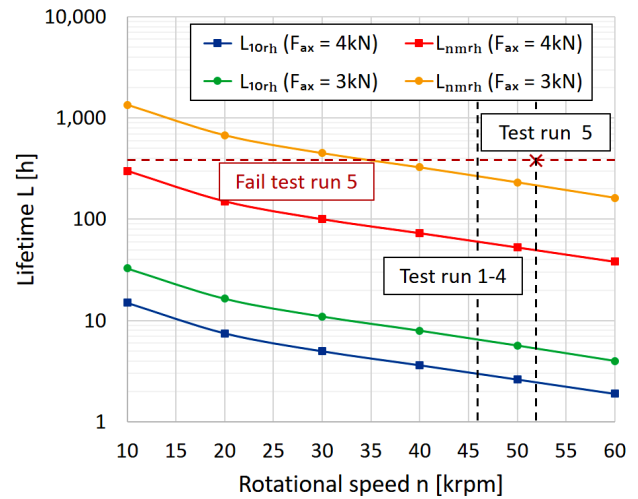

Figure 14. Lifetime calculation for varying rotational speeds

The actual lifetime of test runs 1 – 4 is above the calculated values, as all tests were successfully completed. The failed test run 5 is also above the expected values of the standard with around 400 h runtime. Even though the calculated lifetimes are only design values and do not necessarily reflect the real results, they nevertheless illustrate the extreme operational conditions that the hybrid bearings with raceways made of nitriding steels can withstand.

4. Conclusion

The operational characteristics of hybrid spindle bearings, with raceways made of nitriding steel, were investigated under high loads and speeds. The performance of the bearings was validated based on the outer ring temperature and the vibration values in the test rig. The test runs 1 – 4 at 46 krpm, corresponding to a speed parameter of 2.5 million nd_m and an axial load of 3 kN were successfully completed under stable temperature and vibration conditions. The vibration velocities of these tests are all below the limits of the vibration standard ISO 10816-3. In a sample test (test run 5) for an increased speed of 52 krpm, corresponding to a speed parameter of 2.8 million nd_m and 4 kN axial load, the performance limits of this bearing type could be determined, which failed after 400 h. The calculated analysis of the operational conditions shows that the bearings can run in endurance under supercritical contact stresses compared to standard bearings. Due to the high speeds and loads, the raceways on the inner and outer ring are highly energetically stressed, but the microscope analyses after the tests do not reveal any significant wear. Furthermore, the microscope

view of the raceways of the first bearing pair after the test indicates that they have good micropitting resistance. The comparison of the test results with the calculated lifetimes based on the technical specification ISO/TS 16281 also shows that such a long operation of the bearings would not have been expected under these conditions, which can be attributed to the improved material properties due to the tested bearing steel. For further illustration of the superiority of the adhesive wear resistance of the nitriding raceway steels, further tests are planned at higher loads and speeds, which will then be compared in tests with the conventional bearings.

Acknowledgement

References

[1] S. Thakur, K.K. Thakur, H. Singh, Review paper on machinability of titanium alloys, AGU International Journal of Engineering & Technology, Vol. 4, 2017, pp. 70-79.

[2] C. Brecher, M. Weck, Machine Tools Production Systems 2, Springer, Berlin, 2021, DOI: 10.1007/978-3-662-60863-0

[3] SKF super-precision bearings, available at: https://cdn.skfmediahub.skf.com/api/public/0901d19680495562, accessed: 07.03.2023.

[4] G.E. Morales-Espejel, A. Gabelli, Rolling bearing seizure and sliding effects on fatigue life, Proceedings of the Institution of Mechanical Engineers, Part J: Journal of Engineering Tribology, Vol. 233, No. 2, 2019, pp. 339-354, DOI: 10.1177/1350650118779174

[5] G.E. Morales-Espejel, A. Gabelli, Rolling bearing performance rating parameters: Review and engineering assessment, Proceedings of the Institution of Mechanical Engineers, Part C: Journal of Mechanical Engineering Science, Vol. 234, No. 15, 2020, pp. 3064-3077, DOI: 10.1177/0954406220911395

[6] A. Gabelli, J. Lai, T. Lund, K. Rydén, I. Strandell, G.E. Morales-Espejel, The fatigue limit of bearing steels – Part II: Characterization for life rating standards, International Journal of Fatigue, Vol. 38, 2012, pp. 169-180, DOI: 10.1016/j.ijfatigue.2011.12.006

[7] M.Y. Sherif, V. Brizmer, R. Meeuwenoord, C. Matta, E. Broitman, T. Nuijten, The influence of steel microstructure in high-speed high-load bearing applications, Materials Science and Technology, Vol. 37, No. 17, 2021, pp. 1370-1385, DOI: 10.1080/02670836.2021.2010016

[8] G.E. Morales-Espejel, V. Brizmer, Effect of materials and surfaces on frictional heating resistance of high-speed high-load rolling bearings, Proceedings of the Institution of Mechanical Engineers, Part J: Journal of Engineering Tribology, Vol. 236, No. 4, 2022, pp. 583-594, DOI: 10.1177/1350650121102407

[9] C. Brecher, S. Neus, M. Gaertner, L. Catana, F. Greco, G. Morales-Espejel, D. Lang, New bearing steel for high-speed applications, MM Science Journal, 2021, pp. 5334-5339, DOI: 10.17973/MMSJ.2021_12_2021129

[10] M.A. Ragen, D.L. Anthony, R.F. Spitzer, A comparison of the mechanical and physical properties of contemporary and new alloys for aerospace bearing applications, in J.M. Beswick (Ed.), Bearing Steel Technology, ASTM International, West Conshohocken, 2002, pp. 362-374, DOI: 10.1520/STP10866S

[11] O. Bayer, T. Silverio, Increased performance of high speed spindle bearings, in Proceedings of the II International Seminar on Improving Machine Tool Performance, 03-05.07.2000, La Baule-Escoublac, France, Paper B21.

[12] D. Girodin, Deep nitrided 32CrMoV13 steel for aerospace bearings applications, NTN Technical Review, No. 76, 2008, pp. 24-31.

[13] O. Beer, Nitriding of rolling contact races, HTM Journal of Heat Treatment and Materials, Vol. 74, No. 5, 2019, pp. 317-330, DOI: 10.3139/105.110392

[14] ISO 492, Rolling Bearings – Radial Bearings – Geometrical Product Specifications (GPS) and Tolerance Values, 2014.

[15] E. Rolinski, M. Woods, The benefits of nitriding and nitrocarburizing, available at: https://www.machinedesign.com/materials/article/21836791/the-benefits-of-nitriding-and-nitrocarburizing, accessed: 28.07.2023.

[16] J.M. Beswick, Fracture and fatigue crack propagation properties of hardened 52100 steel, Metallurgical Transactions A, Vol. 20, No. 10, 1989, pp. 1961-1973, DOI: 10.1007/BF02650283

[17] Böhler V361 datasheet, available at: https://www.bohler-edelstahl.com/app/uploads/sites/92/2023/07/productdb/api/v361_en.pdf, accessed: 26.07.2023.

[18] DIN EN ISO 683-17, Für eine Wärmebehandlung bestimmte Stähle, legierte Stähle und Automatenstähle – Teil 17: Wälzlagerstähle [Heat-Treated Steels, Alloy Steels and Free-Cutting Steels – Part 17: Ball and Roller Bearing Steels], 2015 [in German].

[19] DIN EN ISO 4957, Werkzeugstähle [Tool Steels], 2018 [in German].

[20] G. Pantazopoulos, P. Psyllaki, An overview on the tribological behaviour of nitro-carburised steels for various industrial applications, Tribology in Industry, Vol. 37, No. 3, 2015, pp. 299-308.

[21] K.A. Widi, I. Wardana, W. Suprapto, Y.S. Irawan, The role of diffusion media in nitriding process on surface layers characteristics of AISI 4140 with and without hard chrome coatings, Tribology in Industry, Vol. 38, No. 3, 2016, pp. 308-317.

[22] J. Falker, Analyse des Betriebsverhaltens von Hochgeschwindigkeits-Wälzlagern unter radialen Lasten [Analysis of the Operating Behavior of High-Speed Rolling Element Bearings under Radial Loads], PhD thesis, RWTH Aachen University, Aachen, 2019 [in German].

[23] ISO 4406, Hydraulic Fluid Power – Fluids – Method for Coding the Level of Contamination by Solid Particles, 2021.

[24] E. Desnica, A. Ašonja, L. Radovanović, I. Palinkaš, I. Kiss, Selection, dimensioning and maintenance of roller bearings, in D. Blažević, N. Ademović, T. Barić, J. Cumin, E. Desnica (Eds.), 31st International Conference on Organization and Technology of Maintenance (OTO 2022), Springer, Cham, 2023, pp. 133-142, DOI: 10.1007/978-3-031-21429-5_12

[25] SKF maintenance and lubrication products, available at: https://cdn.skfmediahub.skf.com/api/public/094fe398236d3d0a/pdf_preview_medium/094fe398236d3d0a_pdf_preview_medium.pdf, accessed: 26.07.2023.

[26] R. Riddell, How to manage hot bearings in your plant, Machinery Lubrication, Vol. 16, No. 5, 2016, pp. 8-12.

[27] ISO 10816-3, Mechanical Vibration – Evaluation of Machine Vibration by Measurements on Non-rotating Parts – Part 3: Industrial Machines with Nominal Power above 15 kW and Nominal Speeds between 120 r/min and 15 000 r/min when Measured in Situ, 2009.

[28] C. de Castelbajac, M. Ritou, S. Laporte, B. Furet, Monitoring of distributed defects on HSM spindle bearings, Applied Acoustics, Vol. 77, 2014, pp. 159-168, DOI: 10.1016/j.apacoust.2013.07.008

[29] C. Brecher, D. Christoffers, S. Neus, Dynamische schmierzustandserkennung öl-luft-geschmierter spindellager [Dynamic lubrication state detection of oil-air-lubricated spindle bearings], Zeitschrift für wirtschaftlichen Fabrikbetrieb, Vol. 115, No. 5, 2020, pp. 327-330, DOI: 10.3139/104.112293 [in German].

[30] C. Brecher, J. Falker, M. Fey, Simulation schnelldrehender wellen-lager-systeme − Teil 1 [Simulation of Fast Rotating Shaft-Bearing Systems − Part 1], Antriebstechnik, Vol. 58, No. 6, 2019, pp. 66-72 [in German].

[31] R. Gohar, H. Rahnejat, Fundamentals of Tribology, Imperial College Press, London, 2008, DOI: 10.1142/p553

[32] T.A. Harris, M.N. Kotzalas, Essential Concepts of Bearing Technology, CRC Press, Boca Raton, 2007.

[33] D.E. Brewe, B.J. Hamrock, Simplified solution for elliptical-contact deformation between two elastic solids, Journal of Lubrication Technology, Vol. 99, No. 4, 1977, pp. 485-487, DOI: 10.1115/1.3453245

[34] R. Gohar, Elastohydrodynamics, Imperial College Press, London, 2001, DOI: 10.1142/p146

[35] ISO 281, Rolling Bearings – Dynamic Load Ratings and Rating Life, 2007.

[36] T.A. Harris, M.N. Kotzalas, Advanced Concepts of Bearing Technology, CRC Press, Boca Raton, 2007.

[37] ISO/TS 16281, Rolling Bearings – Methods for Calculating the Modified Reference Rating Life for Universally Loaded Bearings, 2008.

[38] A.A. Patil, S.S. Desai, L.N. Patil, S.A. Patil, Adopting artificial neural network for wear investigation of ball bearing materials under pure sliding condition, Applied Engineering Letters, Vol. 7, No. 2, 2022, pp. 81-88, DOI: 10.18485/aeletters.2022.7.2.5

[39] A. Gabelli, G.E. Morales-Espejel, A model for hybrid bearing life with surface and subsurface survival, Wear, Vol. 422-423, 2019, pp. 223-234, DOI: 10.1016/j.wear.2019.01.050